A&A 552, A43 (2013)
DOI: 10.1051/0004-6361/201221006

Astronomy & Astrophysics

The Canada-France High-z Quasar Survey: 1.2 mm observations *(Research Note)*

A. Omont[1,2], C. J. Willott[3], A. Beelen[4], J. Bergeron[1,2], G. Orellana[5,4], and P. Delorme[6]

[1] UPMC Univ Paris 06, UMR 7095, Institut d'Astrophysique de Paris, 75014 Paris, France
e-mail: omont@iap.fr
[2] CNRS, UMR 7095, Institut d'Astrophysique de Paris, 75014 Paris, France
[3] Herzberg Institute of Astrophysics, National Research Council, 5071 West Saanich Rd, Victoria, BC V9E 2E7, Canada
[4] Univ Paris-Sud and CNRS, Institut d'Astrophysique Spatiale, UMR 8617, 91405 Orsay, France
[5] Astronomy DepartmentUniversidad de Concepción, Casilla 160-C Concepción, Chile
[6] UJF-Grenoble 1/CNRS-INSU, Institut de Planétologie et d'Astrophysique de Grenoble (IPAG) UMR 5274, 38041 Grenoble, France

Received 25 December 2012 / Accepted 27 January 2013

ABSTRACT

We report 250 GHz (1.2 mm) observations of a sample of 20 quasars at redshifts $5.8 < z < 6.5$ from the Canada-France High-z Quasar Survey (CFHQS), using the Max-Planck-Millimeter-Bolometer (MAMBO) array at the 30-metre telescope of the Institut de Radioastronomie Millmétrique (IRAM). An rms sensitivity of $\lesssim$0.6 mJy was achieved for 65% of the sample, and of $\lesssim$1.0 mJy for 90%. Only one quasar, CFHQS J142952+544717, was robustly detected with $S_{250\,\mathrm{GHz}} = 3.46 \pm 0.52$ mJy. This indicates that one of the most powerful known starbursts at $z \sim 6$ is associated with this radio-loud quasar. On average, the other CFHQS quasars, which have a mean optical magnitude fainter than the previously studied samples of $z \sim 6$ quasars of the Sloan Digital Sky Survey (SDSS), have a mean 1.2 mm flux density $\langle S_{250\,\mathrm{GHz}} \rangle = 0.41 \pm 0.14$ mJy; this average detection with a signal-to-noise (S/N) ratio of 2.9 is hardly meaningful. It would correspond to $\langle L_{\mathrm{FIR}} \rangle \approx 0.94 \pm 0.32 \times 10^{12}\,L_{\odot}$, and an average star formation rate of a few 100 $M_{\odot}$/yr, depending on the stellar initial mass function (IMF) and a possible contribution of an active galactic nucleus (AGN) to $\langle L_{\mathrm{FIR}} \rangle$. This is consistent with previous findings of Wang et al. on the far-infrared emission of $z \sim 6$ quasars and extends their results toward optically fainter sources.

Key words. galaxies: high-redshift – galaxies: starburst – galaxies: active – infrared: galaxies – submillimeter: galaxies

1. Introduction

The highest-redshift quasars which are known at $z \gtrsim 6$ are fascinating objects that provide crucial clues about the growth of supermassive black holes (SMBH), their host galaxies, and their environment toward the end of the reionization epoch when the Universe was less than 1 Gyr old. Black holes of several $10^9\,M_{\odot}$ were already in place (Willott et al. 2003; Kurk et al. 2007; Jiang et al. 2007; Mortlock et al. 2012). Such a rapid growth of the mass of early black holes puts extremely severe constraints on classical Eddington accretion limited by radiation pressure. It might point to the existence of a more efficient process for forming a massive black hole such as direct collapse without fragmenting (Begelman et al. 2006; Volonteri 2012).

In this context, it is obviously critical to accumulate more information about SMBH growth and the parallel formation of the first massive galaxies in the most massive dark matter halos at the reionization epoch. An important point to clarify is the black-hole-to-galaxy mass ratio at this epoch, and to see how it compares to the current value at $z = 0$. A related piece of information is provided by the relationship between the galaxy growth by star formation and the quasar luminosity generated in black hole accretion. Both processes result mainly from gas transport to the center of the galaxy. They should contribute in building the final tight relation between the masses of the black hole and the galaxy, even if this relation is mainly ruled by quasar feedback onto the interstellar gas.

As the emission of young stars is mostly channeled into the far-infrared (FIR) by dust in such massive starburst galaxies, the FIR luminosity, L_{FIR}, directly reflects the star formation rate (SFR). In the absence of multi-wavelength sampling of the FIR emission, one may assume a standard infrared spectral energy distribution (SED) (e.g., Wang et al. 2008), and thus directly derive L_{FIR} and SFR from the measurement of the continuum flux density at a single wavelength. At $z \gtrsim 6$, a single continuum observation in the $\lambda \sim 1$ mm window efficiently probes the bulk of the rest-frame FIR emission and thus provides a simple estimate of L_{FIR} and SFR. In addition, these ~1 mm observations yield valuable estimates of the dust mass in the host galaxy which reflects a combination of the gas mass and the metallicity.

After a series of such mm/submm studies of FIR properties of $z \sim 2$–4 quasars (e.g., Omont et al. 2001, 2003; Carilli et al. 2001; Priddey et al. 2003), this method was successfully applied by Wang et al. (2008, 2011a) to investigate the FIR properties, inferred from 1.2 mm observations, of 40 $z \sim 6$ quasars mainly discovered from the Sloan Digital Sky Survey (SDSS, Fan et al. 2006). A significant percentage (30%) of the Wang et al. $z \sim 6$ sample is detected at 1.2 mm, pointing to an excess of FIR emission dominated by a strong starburst with a star formation rate $\approx$500–1000 $M_{\odot}$/yr. At the sensitivity of these studies, ~1–1.5 mJy at 1.2 mm, 70% of the quasars are not detected, and for the whole sample the behavior of the FIR luminosity with respect to the bolometric luminosity L_{bol} is similar to that of all

Table 1. Optical data and results of 1.2 mm observations of full CFHQS sample.

Name	RA	Dec	Redshift[†]	m_{1450}[*]	M_{1450}[#]	$L_{\rm bol}$ ($10^{13}\,L_\odot$)	$S_{250\ \rm GHz}$ (mJy)	$z'_{\rm AB}$
CFHQS J003311−012524	00:33:11.40	−01:25:24.9	6.13	21.53	−24.91	0.94	1.13 ± 0.36	22.41 ± 0.08
CFHQS J005006+344522	00:50:06.67	+34:45:22.6	6.253	19.84	−26.65	4.67	0.69 ± 0.76	20.47 ± 0.03
CFHQS J005502+014618	00:55:02.91	+01:46:18.3	5.983	21.82	−24.55	0.68	0.43 ± 0.46	22.19 ± 0.06
CFHQS J010250−021809	01:02:50.64	−02:18:09.9	5.95	22.02	−24.34	0.56	1.01 ± 0.38	22.30 ± 0.08
CFHQS J013603+022605	01:36:03.17	+02:26:05.7	6.21	22.04	−24.43	0.61	1.18 ± 0.97	22.10 ± 0.09
CFHQS J021013−045620	02:10:13.19	−04:56:20.9	6.4323	22.25	−24.31	0.70	1.14 ± 0.93	22.67 ± 0.05
CFHQS J021627−045534	02:16:27.81	−04:55:34.1	6.01	24.15	−22.24	0.08	0.37 ± 0.57	24.40 ± 0.06
CFHQS J022122−080251	02:21:22.71	−08:02:51.5	6.161	21.98	−24.47	0.63	−1.48 ± 1.36	22.63 ± 0.05
CFHQS J022743−060530	02:27:43.29	−06:05:30.2	6.20	21.41	−25.05	1.08	−0.03 ± 0.53	22.71 ± 0.06
CFHQS J031649−134032	03:16:49.87	−13:40:32.2	5.99	21.72	−24.66	0.75	2.76 ± 1.44	21.72 ± 0.08
CFHQS J105928−090620	10:59:28.61	−09:06:20.4	5.92	20.75	−25.60	1.79	0.03 ± 0.82	20.82 ± 0.03
CFHQS J142952+544717	14:29:52.17	+54:47:17.6	6.1831	20.59	−25.88	2.31	3.46 ± 0.52	21.45 ± 0.03
CFHQS J150941−174926	15:09:41.78	−17:49:26.8	6.121	19.63	−26.80	5.41	0.91 ± 0.47	20.26 ± 0.02
CFHQS J164121+375520	16:41:21.64	+37:55:20.5	6.047	21.19	−25.21	1.25	0.25 ± 0.47	21.31 ± 0.04
CFHQS J210054−171522	21:00:54.62	−17:15:22.5	6.087	21.37	−25.05	1.08	0.29 ± 0.59	22.35 ± 0.09
CFHQS J222901+145709	22:29:01.65	+14:57:09.0	6.152	21.90	−24.55	0.68	0.82 ± 0.80	22.03 ± 0.05
CFHQS J224237+033421	22:42:37.55	+03:34:21.6	5.88	22.09	−24.25	0.51	0.72 ± 0.61	21.93 ± 0.04
CFHQS J231802−024634	23:18:02.80	−02:46:34.0	6.05	21.55	−24.85	0.90	0.54 ± 0.56	21.66 ± 0.05
CFHQS J232908−030158	23:29:08.28	−03:01:58.8	6.417	21.53	−25.02	1.05	0.06 ± 0.50	21.76 ± 0.05
CFHQS J232914−040324	23:29:14.46	−04:03:24.1	5.90	21.96	−24.39	0.58	−1.45 ± 0.63	21.87 ± 0.08

Notes. [(†)] Redshifts are from Willott et al. (2007, 2009, 2010a,b, 2013); Wang et al. (2011b). Redshifts to 4 decimal places are from millimeter lines, those to 3 decimal places from broad UV MgII lines, and those to 2 decimal places from Ly-α. [(*)] Apparent magnitude at rest-frame 1450 Å. [(#)] Absolute magnitude at rest-frame 1450 Å. The values given here supersede previously published values of M_{1450}. They were derived by fitting a typical quasar spectrum to the observed J-band magnitudes.

quasars at any redshift, pointing to an important contribution of the active galactic nuclei (AGN) to the FIR emission.

Besides SDSS, the Canada-France High-z Quasar Survey (CFHQS) is the second largest provider of $z \sim 6$ quasars. With 20 sources it accounts for about one third of the total number of quasars at $5.7 < z < 6.5$. Coming from deeper optical surveys, the CFHQS sample contains quasars optically much fainter than both the main SDSS sample and the SDSS deep southern survey. The purpose of this Note is to publish the results of the 1.2 mm survey of the 20 $z \sim 6$ CFHQS quasars that we performed to extend the existing studies of FIR properties of quasars at similar redshifts to optically fainter sources. For four of these sources, 1.2 mm results were already published in Willott et al. (2007). The exceptionally strong 1.2 mm flux density that we found for CFHQS J1429+5447 led to the selection of this source to search for CO(2−1) emission (Wang et al. 2011b). Together with those of Wang et al. (2011a), our results provide a useful background for the much deeper studies of submillimeter properties of optically faint $z \sim 6$ quasars that we have already begun with The Atacama Large Millimeter/submillimeter Array (ALMA, Willott et al. 2013).

Cosmological parameters of $H_0 = 70$ km s^{-1} Mpc^{-1}, $\Omega_{\rm M} = 0.28$ and $\Omega_\Lambda = 0.72$ (Komatsu et al. 2009) are assumed throughout.

2. Observations

The CFHQS is an optically-selected survey for $5.8 < z < 6.5$ quasars. It was carried out in regions of the sky observed as part of the Canada-France-Hawaii Telescope Legacy Survey[1], the Subaru/*XMM-Newton* Deep Survey and the Red-sequence Cluster Survey 2. With $z'_{\rm AB}$-band magnitude survey limits ranging from $z'_{\rm AB} = 22$ to $z'_{\rm AB} = 24.5$ in different regions of the sky, CFHQS quasars are typically 10−100 times lower in luminosity than quasars at the same redshift from the main SDSS sample (Fan et al. 2006), and many are less luminous than those from the SDSS Deep Stripe (Jiang et al. 2008, 2009). The CFHQS survey contains 20 spectroscopically-confirmed quasars at $5.88 < z < 6.43$, a significant percentage of the total of ≈60 quasars known at this epoch (Willott et al. 2007, 2009, 2010a,b). Table 1 contains the positions, redshifts, magnitudes, absolute magnitudes and bolometric luminosities of the full sample. Bolometric luminosities have been determined from the absolute magnitudes at 1450 Å assuming a bolometric conversion factor $\zeta_{1450\rm A} = L_{\rm bol}/(\nu L_{\nu,1450\rm A})$ of 4.4 (Richards et al. 2006).

The millimeter observations were performed within the pool observing sessions at the IRAM 30 m telescope in the winters of 2007 through 2010 using the 117-element version of the Max Planck Millimeter Bolometer (MAMBO) array (Kreysa et al. 1998) operating at an average wavelength of 1.2 mm (250 GHz). We used the standard on-off photometry observing mode, chopping between the target and sky by 32″ in azimuth at 2 Hz every 10 s, and nodding the telescope every 10 or 20 s (see e.g., Wang et al. 2011a). On average, the noise of the channel used for point-source observations was about 35−40 mJy $\sqrt{\rm s}$/beam. This allowed us to achieve rms $\lesssim$0.5−1.0 mJy for 18 of the 20 sources, with 0.5−1.5 hr of telescope time per source. Unfortunately, poor weather conditions during the last observing runs prevented us from reaching the aimed rms of ∼0.6 mJy for 8 sources out of 20. The data were reduced with standard procedures to minimize the sky noise with the package developed by Zylka (1998).

The results are shown in Table 1. Only the peculiar source CFHQS J1429+5447 is detected with a signal-to-noise ratio $S/N > 5$. Two other sources, CFHQS J0033-0125 (Willott et al. 2007) and CFHQS J0102-0218, are marginally detected with $S/N = 3.1$ and 2.7, respectively, thanks to special deeper observations that bring the rms below 0.4 mJy. There are ten other

[1] http://www.cfht.hawaii.edu/Science/CFHTLS

Table 2. Average properties.

Group	Number	$\langle L_{\rm bol}\rangle^{\rm av*}$ ($10^{13}\,L_\odot$)	$\langle L_{\rm bol}\rangle^{\rm med*}$ ($10^{13}\,L_\odot$)	$\langle S_{250\ \rm GHz}\rangle^{\dagger}$ (mJy)	$\langle L_{\rm FIR}\rangle^{\dagger\dagger}$ ($10^{12}\,L_\odot$)	$\langle M_{\rm dust}\rangle^{\dagger\dagger}$ ($10^{8}\,M_\odot$)
a) All objects	20	1.31	0.90	0.63 ± 0.14	1.45 ± 0.32	0.58
b) Homogeneous	18	1.38	0.94	0.64	1.46	0.59
c) Regular	19	1.26	0.75	0.41 ± 0.14	0.94 ± 0.32	0.38
d) 250 GHz-undetected	17	1.32	0.75	0.34 ± 0.15	0.78 ± 0.34	0.31
e) Regular $m_{1450} < 21.7$	9	2.02	1.08	0.42 ± 0.19	0.96 ± 0.44	0.39
f) Regular $m_{1450} > 21.7$	10	0.58	0.63	0.41 ± 0.22	0.94 ± 0.51	0.38
CFHQS J1429+5447[#]	1	2.31		3.46 ± 0.52	7.85 ± 1.18	3.16
CFHQS J0033-0125	1	0.94		1.13 ± 0.36	2.58 ± 0.82	1.04
CFHQS J0102-0218	1	0.56		1.01 ± 0.38	2.35 ± 0.89	0.95

Notes. [(*)] Bolometric luminosity: [av] mean value (straight average, with equal weight for all sources); [med] median value. [(†)] Averages of $S_{250\ \rm GHz}$ are performed as described in Sect. 3.2: groups a to f. (a): Whole sample, regularized rms weighted average. (b): All objects except CFHQS J0221−802 and CFHQS J0316−1340 whose 250 GHz rms are peculiarly large; straight average (with equal weight for all sources). (c): All objects except CFHQS J1429+5447 which is exceptionally strong at 250 GHz and radio loud (Sect. 3.2); regularized rms. (d): All objects except CFHQS J0033-0125, CFHQS J0102-0218, and CFHQS J1429+5447 which are (tentatively) detected; regularized rms. (e): Same as c), but $m_{1450} < 21.7$. (f): Same as c), but $m_{1450} > 21.7$. [(#)] The value used for $L_{\rm FIR}$ of CFHQS J1429+5447 corresponds to the totality of the measured 250 GHz flux density, while only an unknown part is emitted by the starburst dust in the quasar host galaxy. [(††)] $\langle L_{\rm FIR}\rangle$ is inferred from $\langle S_{250\ \rm GHz}\rangle$ through Eq. (1) (for all groups with several sources, the average redshift $\langle z\rangle = 6.09$ is assumed); $\langle M_{\rm dust}\rangle$ is inferred from $\langle L_{\rm FIR}\rangle$ through Eq. (2).

sources with rms between 0.45 and 0.65 mJy, and five between 0.75 and 1.0 mJy, all with $S/N < 2$.

This 3σ detection rate of barely 10% is significantly smaller than that of Wang et al. (2011a) who report a rate of 30%. This difference may be partially due to our lower sensitivity – average rms 0.69 mJy instead of 0.52 mJy for the Wang et al. sources with $m_{1450} > 20.2$. However, there is certainly also an effect of the larger bolometric luminosities of their sample, as discussed in Sect. 4.

3. Far-infrared luminosities

3.1. Estimates of L_{FIR} and M_{dust}

One may convert the 250 GHz flux densities - corresponding to $\lambda_{\rm rest} \sim 170\,\mu$m – to FIR luminosities by assuming a model for the FIR SED. For homogeneity, we take the same assumptions as Wang et al. (2008, 2011a) for this SED, i.e. assume an optically thin graybody with a dust temperature of $T_{\rm d} = 47$ K and emissivity index of $\beta = 1.6$. As proposed by Beelen et al. (2006), these are typical values for the FIR luminous quasars at $z \sim 2$–4. We also select the same wavelength range, 42.5–122.5 μm, for the definition of the FIR luminosity as Wang et al. (2008, 2011a). Values of $L_{\rm FIR}$ thus calculated for detected or tentatively detected sources are reported in Table 2. For the average redshift of our sample, $\langle z\rangle = 6.09$, the conversion factor between the average values of the 250 GHz flux density and $L_{\rm FIR}$ is

$$\langle L_{\rm FIR}\rangle/10^{12}\,L_\odot = 2.30 \times \langle S_{250\ \rm GHz}\rangle({\rm mJy}). \quad (1)$$

For other redshifts the conversion factor is slightly different, varying from 2.35 for $z = 5.88$ to 2.16 for $z = 6.43$. However, we note that our faint sources have much lower mm fluxes than the typical sources used to determine the dust temperature value $T_{\rm d} = 47$ K. If our sources instead have parameters closer to those of nearby luminous infrared galaxies (LIRGs, 10^{11}–$10^{12}\,L_\odot$, $T_{\rm d} \approx 33$ K, U et al. 2012), then the values of $L_{\rm FIR}$ would be ∼3 times lower for $T_{\rm d} = 33$ K.

The dust mass $M_{\rm dust}$ at $T_{\rm dust}$ is related to the FIR luminosity by $M_{\rm dust} = L_{\rm FIR}/4\pi \int \kappa_\nu B_\nu {\rm d}\nu$, where B_ν is the Planck function and $\kappa_\nu = \kappa_0(\nu/\nu_0)^\beta$ is the dust absorption coefficient. Using $\kappa_0 = 18.75\,{\rm cm^2\,g^{-1}}$ at 125 μm (Hildebrand 1983) as do Wang et al. (2008, 2011a), yields

$$M_{\rm dust}/10^8\,M_\odot = 0.40 \times L_{\rm FIR}/10^{12}\,L_\odot. \quad (2)$$

For $T_{\rm d} = 33$ K, the values of $M_{\rm dust}$ would be ∼7 times larger than for $T_{\rm d} = 47$ K for the same $L_{\rm FIR}$ (∼2.4 times larger for the same $S_{250\ \rm GHz}$).

3.2. Average FIR luminosities

Considering the small number of 1.2 mm detections, we use the additional information provided by the averages derived from various stacking of the observed 1.2 mm flux densities. However, some care must be taken in calculating these averages because of the inhomogeneity of our data. Because the redshift range of our sample is small, it is simpler to perform all the averages on the 1.2 mm flux density, $S_{250\ \rm GHz}$, and to infer the corresponding average of $L_{\rm FIR}$ by using the conversion factor of Eq. (1) for the average redshift 6.09. We will consider the following various averages of $S_{250\ \rm GHz}$:

- a) Classical rms weighted averages with weights proportional to $1/{\rm rms}^2$. However, this could give too much weight to the two sources with rms <0.4 mJy whose integration time was anomalously long. It seems better to replace their rms by a typical value – median of the rms of the other sources (regularized rms).
- b) Plain, straight average of the nominal values of $S_{250\ \rm GHz}$ with equal weights irrespective of the rms. However, this does not take into account the difference in quality of these values. Therefore, we give the result of this straight average in Table 2 discarding the two sources whose 250 GHz rms are peculiarly large.
- c) As there is clearly one exceptional source, CFHQS J1429+5447, which is more than three times stronger at 1.2 mm than all the others, and is radio loud (Sect. 3.3), one may prefer to exclude it, stacking only the 19 other sources with weights as in a).
- d) One might also exclude the two other tentative detections, stacking only 17 sources with weights as in a).

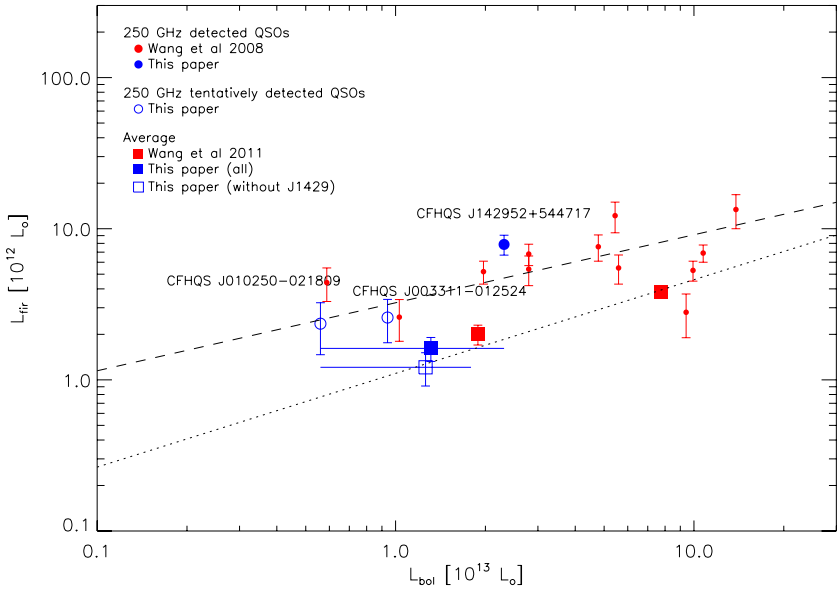

Fig. 1. Similar to Fig. 4 of Wang et al. (2011a). FIR and bolometric luminosity correlations of $z \sim 6$ quasars, showing: 1) average luminosities (large symbols) for: 1a) our whole sample of 20 sources and that of 19 sources taking out CFHQS J1429+5447 (the horizontal error bars contain 80% of the data points of these samples, excluding the two highest and lowest values of $L_{\rm bol}$); 1b) average values of Wang et al. (2011a) for optically faint ($m_{1450} \geq 20.2$) and bright ($m_{1450} < 20.2$) sources; 2) individual luminosities (small symbols) for our 250 GHz detections and tentative detections, together with the detections of Wang et al. (2008) for comparison. Note that for CFHQS J1429+5447, the value used for $L_{\rm FIR}$ corresponds to the totality of the measured 250 GHz flux density, while only an unknown part is emitted by the starburst dust in the quasar host galaxy. The two straight lines are reproduced from Fig. 4 of Wang et al. (2011a): the dotted line [$\log(L_{\rm FIR}) = 0.62 \log(L_{\rm bol}) + 3.9$] is a power-law fit to the average luminosities of all the quasar high-z samples, and the dashed line [$\log(L_{\rm FIR}) = 0.45 \log(L_{\rm bol}) + 6.6$] shows the power-law fit to the sub-millimeter- or millimeter-detected quasars in all high-z samples and local ultra-luminous infrared galaxies (ULIRGs). To be consistent with our selected bolometric conversion factor $\zeta_{1450\rm A} = 4.4$ (Sect. 2), we have scaled all the values used by Wang et al. for $L_{\rm bol}$ using our bolometric conversion factor instead of $\zeta_{1450\rm A} \approx 6$ which we inferred from Table 4 and Fig. 4 of Wang et al. (2011a).

– e) and f) One may try to split the sample into two halves with respect to the UV luminosity to see whether the UV luminosity can have some visible effect on $\langle S_{250\ \rm GHz} \rangle$.

In Table 2, we give the results corresponding to all these options. It is seen that the results of the first two do not differ significantly. As expected, dropping CFHQS J1429+5447 leads to a decrease of the average flux density, yielding $\langle S_{250\ \rm GHz} \rangle = 0.41 \pm 0.14$ for the rms weighted average of the 19 other sources. This is probably the best average for the most representative sources of our sample, but at 2.9σ it is hardly meaningful. In addition, small residual systematic errors in MAMBO results are not excluded at this level.

Note that the average of $\log(L_{\rm FIR})$ (or $S_{250\ \rm GHz}$) for groups e) and f) is found to be about the same even though these groups are split by luminosity. This may appear surprising because one may expect to see a decrease of $\langle L_{\rm FIR} \rangle$ with $\langle L_{\rm bol} \rangle$ in line with the results of Wang et al. (2011a, see lower dotted line in Fig. 1). However this can be easily explained by the fact that we do not have a huge luminosity range in our sample. The average $\langle L_{\rm bol} \rangle$ of these groups differ by a factor of 4 and the medians less than a factor of 2. Given that each stack is detected at only $S/N \sim 2$, our results are consistent with the relation of Wang et al.

3.3. CFHQS J142952.17+544717.6

This quasar is the only one detected at 1.2 mm with a high S/N ratio, $S_{250\ \rm GHz} = 3.46 \pm 0.52$ mJy. The corresponding values of the FIR luminosity and the dust mass are reported in Table 2. Besides being one of the mm-brightest $z \sim 6$ quasars and one of the UV most luminous of our sample, it is remarkable in many other respects. It is one of the only four known radio-loud $z \sim 6$ quasars (see e.g., Frey et al. 2011) and has the highest redshift and strongest radio emission among them. The Extended Very Large Array (EVLA) observation of its CO(2−1) line (Wang et al. 2011b), prompted by our 1.2 mm result, has shown a strong CO emission resolved in two peaks, one on top of the quasar position and the other 1.2″ away. Each corresponds to a gas mass larger than $10^{10}\ M_\odot$. The value of the ratio of the FIR to CO luminosities, $L_{\rm FIR}/L'_{\rm CO} = 300$, is just below the average of this ratio for the $z \sim 6$ quasars where Wang et al. (2010) have detected CO. This indicates that most of the 1.2 mm continuum emission probably comes from dust and not from the radio source. The radio source is compact and has a very steep radio spectrum (3.03 ± 0.005, 0.99 ± 0.006 and 0.257 ± 0.015 mJy at 1.6, 5, and 32 GHz, respectively; Frey et al. 2011; Wang et al. 2011b). This is another indication that most of the millimeter emission is due to dust, although a significant synchrotron contribution cannot be fully excluded. Moreover, it is not yet known how the observed 250 GHz flux density is shared between the dust emission of each galaxy, and possibly the synchrotron emission of the quasar. Therefore, in Table 2 and Fig. 1 the value of $L_{\rm FIR}$ corresponds to the totality of the measured 250 GHz flux density, while only an unknown part is emitted by the starburst dust in the quasar host galaxy.

4. Discussion and conclusions

The most natural explanation for an excess of FIR emission is star formation. If the FIR emission is powered by a dusty starburst, there is a direct relation between SFR and $L_{\rm FIR}$. The most generally used relation is given by Kennicutt (1998), $SFR(M_\odot/{\rm yr}) = 1.72 \times 10^{-10}\ L_{\rm FIR}(L_\odot)$ for a Salpeter IMF and $8 < \lambda < 1000\,\mu$m. However, the exact

conversion factor significantly depends on the IMF and the selected wavelength range for estimating $L_{\rm FIR}$. With our selected wavelength range, 42.5−122.5 μm, it is conservative to assume that $SFR(M_\odot/{\rm yr}) \gtrsim 1.5 \times 10^{-10}\, L_{\rm FIR}(L_\odot)$.

For sources with large FIR excess, such as CFHQS J1429+5447, it is generally agreed that most of the FIR emission is powered by a starburst (see e.g., Beelen et al. 2006; Wang et al. 2008; Mor et al. 2012). This yields $SFR \gtrsim 500\ M_\odot$/yr for each of the two galaxies of CFHQS J1429+5447. For the other sources, making the assumption that all the FIR emission is due to star formation, the value for group c in Table 2, $\langle L_{\rm FIR}\rangle \approx 0.94 \pm 0.32 \times 10^{12}\ L_\odot$, would imply $SFR \gtrsim 140 \pm 50\ M_\odot$/yr.

For the much smaller FIR emission of the majority of quasars, an important starburst contribution is also likely; however, it is possible that a portion also comes from dust powered by the AGN. This was pointed out for $z \sim 6$ quasars by Wang et al. (2011a). They extended their discussion to lower redshifts and they quote various other authors who also discuss lower redshifts (see also e.g., Rosario et al. 2012; Dai et al. 2012, for more recent references). In their Fig. 4, (partially reproduced in Fig. 1), they have shown that there is a remarkably uniform correlation of $L_{\rm FIR}$ with $L_{\rm bol}$ for quasar average luminosities, both for various samples of high-z quasars, and of low-z ones (e.g., Hao et al. 2005). This correlation is well represented by the power law $[\log(L_{\rm FIR}) = 0.62 \times \log(L_{\rm bol}) + 3.9]$ (see Fig. 1). A starburst contribution is needed to explain the FIR slope of 0.6, while the slopes for IRAS 12 μm and 25 μm of local quasars are linear and consistent with AGN heating (Hao et al. 2005). However, this relatively high value of 0.6 for the FIR slope may be evidence for a combination of AGN and starburst contributions.

In Fig. 1, which is similar to Fig. 4 of Wang et al. (2011a), we show the correlations for our sample between $L_{\rm FIR}$ and $L_{\rm bol}$, computed as described above (Sect. 2). Comparing the plotted average luminosities for all our 20 sources, with and without CFHQS J1429+5447, to the averages of Wang et al. (2011a) for $m_{1450} < 20.2$ and >20.2, shows that our sample represents a significant extension to the work of Wang et al. toward optically weaker sources. Our average for all 20 observed sources, including CFHQS J1429+5447, appears consistent with the two averages of Wang et al. for all the $z \sim 6$ quasars they observed, respectively optically faint and bright. The average for our 19 sources, without CFHQS J1429+5447, is in better agreement with the power-law fit that Wang et al. found for the average luminosities of all the high-z samples of quasars observed in millimeter.

The position of CFHQS J1429+5447 in Fig. 1 is well within the region of 1.2 mm detected sources by Wang et al. (2008, 2011a). Finally in Fig. 1 we have added the positions of the two tentatively detected sources at 1.2 mm, CFHQS J0033−0125 ($S/N = 3.1$) and CFHQS J010250-0218 ($S/N = 2.7$). They are again close to the line fitting mm-detected sources.

In conclusion, our 1.2 mm observations confirm the results of Wang et al. (2011) about the FIR emision of $z \sim 6$ quasars and extend them toward optically fainter sources. The core of our sample is made of faint sources, $21.5 \lesssim z'_{\rm AB} \lesssim 22.7$, corresponding to $L_{\rm bol} \sim (0.5{-}1) \times 10^{13}\, L_\odot$ and black-hole masses of a few $10^8\, M_\odot$ (Willott et al. 2010b). For these quasars, the average FIR luminosity is weak, but probably still significant $\langle L_{\rm FIR}\rangle \approx 0.94 \pm 0.32 \times 10^{12}\, L_\odot$. This corresponds to an average star formation rate of a few 100 $M_\odot$/yr. However, there is certainly a large dispersion for individual sources around these average values − at least a factor ∼3 in both directions, as exemplified by our two tentative 1.2 mm detections, CFHQS J0033−0125 and CFHQS J0102-0218, in this $L_{\rm bol}$ range, and the very low 1.2 mm flux density measured with ALMA for two CFHQS quasars (Willott et al. 2013).

Star-formation rates at such low levels probably reflect the fact that both the gas mass and the total mass of the host galaxy are small. This should then favor large ratios $M_{\rm BH}/M_{\rm galaxy}$, which could be significantly larger than the typical ratio at $z = 0$ ($M_{\rm BH}/M_{\rm bulge} \approx 0.0014$; Marconi & Hunt 2003). But ratios like these remain very uncertain in the absence of direct measurements of $M_{\rm gas}$ and $M_{\rm galaxy}$, e.g., by CO or C^+ observations (e.g., Wang et al. 2011b, 2012; Willott et al. 2013).

Acknowledgements. We thank T. Forveille and X. Delfosse for useful discussions. Based on observations with the IRAM 30 m MRT at Pico Veleta. IRAM is supported by INSU/CNRS (France), MPG (Germany) and IGN (Spain). Thanks to the queue observers at IRAM who obtained data for this paper. Thanks to INSU for the financial support for G. Orellana's visit to France. Based on observations obtained with MegaPrime/MegaCam, a joint project of CFHT and CEA/DAPNIA, at the Canada-France-Hawaii Telescope (CFHT) which is operated by the National Research Council (NRC) of Canada, the Institut National des Sciences de l'Univers of the Centre National de la Recherche Scientifique (CNRS) of France, and the University of Hawaii. This work is based in part on data products produced at TERAPIX and the Canadian Astronomy Data Centre as part of the Canada-France-Hawaii Telescope Legacy Survey, a collaborative project of NRC and CNRS.

References

Beelen, A., Cox, P., Benford, D. J., et al. 2006, ApJ, 642, 694
Begelman, M. C., Volonteri, M., & Rees, M. J. 2006, MNRAS, 370, 289
Carilli, C. L., Bertoldi, F., Rupen, M. P., et al. 2001, ApJ, 555, 625
Dai, Y., Bergeron, J., Elvis, M., et al. 2012, ApJ, 753, 33
Fan, X., Strauss, M. A., Becker, R. H., et al. 2006, AJ, 132, 117
Frey, S., Paragi, Z., Gurvits, L. I., Gabányi, K. É., & Cseh, D. 2011, A&A, 531, L5
Hao, C. N., Xia, X. Y., Mao, S., Wu, H., & Deng, Z. G. 2005, ApJ, 625, 78
Hildebrand, R. H. 1983, Quarterly J. Royal Astron. Soc., 24, 267
Jiang, L., Fan, X., Vestergaard, M., et al. 2007, AJ, 134, 1150
Jiang, L., Fan, X., Bian, F., et al. 2008, AJ, 135, 1057
Jiang, L., Fan, X., Annis, J., et al. 2009, AJ, 138, 305
Kennicutt, R. C., Jr. 1998, ARA&A, 36, 189
Komatsu, E., Dunkley, J., Nolta, M. R., et al. 2009, ApJS, 180, 330
Kreysa, E., Gemuend, H.-P., Gromke, J., et al. 1998, Proc. SPIE, 3357, 319
Kurk, J. D., Walter, F., Fan, X., et al. 2007, ApJ, 669, 32
Marconi, A., & Hunt, L. K. 2003, ApJ, 589, L21
Mor, R., Netzer, H., Trakhtenbrot, B., Shemmer, O., & Lira, P. 2012, ApJ, 749, L25
Mortlock, D. J., Warren, S. J., Venemans, B. P., et al. 2011, Nature, 474, 616
Omont, A., Cox, P., Bertoldi, F., et al. 2001, A&A, 374, 371
Omont, A., Beelen, A., Bertoldi, F., et al. 2003, A&A, 398, 857
Priddey, R. S., Isaak, K. G., McMahon, R. G., & Omont, A. 2003, MNRAS, 339, 1183
Richards, G. T., Lacy, M., Storrie-Lombardi, L. J., et al. 2006, ApJS, 166, 470
Rosario, D. J., Santini, P., Lutz, D., et al. 2012, A&A, 545, A45
U, V., Sanders, D. B., Mazzarella, J. M., et al. 2012, ApJS, 203, 9
Volonteri, M. 2012, Science, 337, 544
Wang, R., Wagg, J., Carilli, C. L., et al. 2008, AJ, 135, 1201
Wang, R., Carilli, C. L., Neri, R., et al. 2010, ApJ, 714, 699
Wang, R., Wagg, J., Carilli, C. L., et al. 2011a, AJ, 142, 101
Wang, R., Wagg, J., Carilli, C. L., et al. 2011b, ApJ, 739, L34
Wang, R., Wagg, J., Carilli, C. L., et al. 2012 [arXiv:1210.0242]
Willott, C. J., McLure, R. J., & Jarvis, M. J. 2003, ApJ, 587, L15
Willott, C. J., Delorme, P., Omont, A., et al. 2007, AJ, 134, 2435
Willott, C. J., Delorme, P., Reylé, C., et al. 2009, AJ, 137, 3541
Willott, C. J., Delorme, P., Reylé, C., et al. 2010a, AJ, 139, 906
Willott, C. J., Albert, L., Arzoumanian, D., et al. 2010b, AJ, 140, 546
Willott, C. J., Omont, A., & Bergeron, J. 2013, ApJ, submitted [arXiv:1302.1587]
Zylka, R. 1998, MOPSI Users Manual (Grenoble: IRAM)